Photoacoustic spectral analysis to sense programmed erythrocyte cell death (eryptosis) for monitoring cancer response to treatment

Muhannad N. Fadhel[1,2,3], Fayruz Kibria[1,2,3], Michael C. Kolios[1,2,3*]

[1] Department of Physics, Ryerson University

[2] Institute for Biomedical Engineering, Science and Technology (iBEST), a partnership between Ryerson University and St. Michael's Hospital

[3] Keenan Research Centre for Biomedical Science of St. Michael's Hospital

[*]mkolios@ryerson.ca

ABSTRACT

Many types of cancer therapies target the tumor microenvironment, causing biochemical and morphological changes in tissues. In therapies using ultrasound activated microbubbles, vascular collapse is typically reported. Red blood cells (RBCs) that leak out of the vasculature become exposed to the ceramide that is released from damaged endothelial cells. Ceramide can induce programmed cell death in RBCs (eryptosis), and is characterized by cell shrinkage, membrane blebbing and scrambling. Since the effect of eryptotic cells on generated photoacoustics (PA) signals has not been reported, we investigated the potential PA may have for cancer treatment monitoring by using PA spectral analysis to sense eryptosis. To induce eryptosis, C2-ceramide was added to RBC suspensions and that were incubated for 24 hours at 37^{o}C. A control and ceramide-induced sample was imaged in a vessel phantom using a high frequency PA system (VevoLAZR, 10 – 45 MHz bandwidth) irradiated with multiple wavelengths ranging from 680 to 900 nm. PA spectral parameters were measured and linked to changes in RBCs as it underwent eryptosis. These samples were examined using optical microscopy, a blood gas analyzer and an integrating sphere setup to measure optical properties (wavelengths 600 – 900 nm). The results of the experiment demonstrate how PA spectral analysis can be used to identify eryptosis at a depth of more than 1 cm into the phantom using ultrasound derived the y-intercept and mid bandfit (MBF) parameters at optical wavelengths of 800 – 900 nm. These parameters were correlated to the morphological and biochemical changes that eryptotic RBCs display. The results establish the potential of PA in cancer treatment monitoring through sensing treatment induced eryptosis.

Keywords: eryptosis, ceramide, cancer therapy, photoacoustics spectral analysis, spectrophotometer, optical properties, blood gas analyzer.

1. INTRODUCTION

Ultrasound activated microbubble have recently been introduced in medical applications as a cancer therapy agent. The synergistic effect of ultrasound activated microbubbles combined with radiation has already been demonstrated [1], [2]. Microbubble shell disruption and gas release induces damage to the endothelial cells lining the vessels, thus resulting in subsequent vessel collapse [3], [4]. The damaged endothelial cells undergo apoptosis which have been shown to rapidly produce ceramide in the process [5]. Ceramide and phosphocholine are produced through the hydrolysis of sphingomyelin (part of the phospholipid bilayer) by acid sphingomyelinase (ASMases). Endothelial cells contain 20 fold more ASMase compared to other mammalian cells, resulting in the dramatic increase of ceramide content at the location of the treatment [6], [7].

Photons Plus Ultrasound: Imaging and Sensing 2016, edited by Alexander A. Oraevsky, Lihong V. Wang
Proc. of SPIE Vol. 9708, 97080O · © 2016 SPIE · CCC code: 1605-7422/16/$18 · doi: 10.1117/12.2211760

Downloaded From: http://proceedings.spiedigitallibrary.org/ on 05/08/2016 Terms of Use: http://spiedigitallibrary.org/ss/TermsOfUse.aspx

The released ceramide interacts with the surrounding red blood cells (RBCs) to signal eryptosis (cell death). Eryptosis is characterized by biochemical and morphological changes in RBCs, through cell shrinkage, membrane blebbing, membrane phospholipid scrambling, leakage of hemoglobin molecules and the conversion of hemoglobin into methemoglobin [8]–[11]. Even though biochemical and morphological changes of eryptotic RBCs have been investigated, how these changes modify photoacoustic (PA) signals warrants investigation.

PA imaging in biomedical imaging is one of the fastest growing modalities as it provides simultaneous structural and functional information [12]–[14]. RBCs contain hemoglobin molecules which are a major contributor to the generation of the PA signals. Changes of individual RBCs at the microscale level in deep tissue are difficult to detect using PA because of the limitations of the imaging system and the small size of RBCs (6 – 8 μm in diameter). However, ultrasound spectral analysis of generated PA signals can serve as a surrogate to sense morphological and biochemical changes to RBCs as they undergo eryptosis.

Ultrasound spectral analysis has been extensively used in analyzing pulse eco ultrasound signals for ultrasound tissue characterization [15]; however, PA spectral analysis is still in its early stages. Spectral analysis refers to parameter extraction from the frequency domain power spectra of the received ultrasound signals. A reference is used to reduce the effect of the transducer to attain system independent parameters [16], [17]. These approaches have provided information about the size and shape of the ultrasound source at scales smaller than the working wavelength of the system [18]–[20]. The information can be related to the dimension, distribution and concertation of the ultrasound sources which, in the case of PA imaging, are RBCs [17]. The effect of eryptosis on generated PA signals have never been investigated and thus the goal of this study is to investigate PA signals generated from RBCs induced by ceramide and compare it to morphological and biochemical changes eryptotic RBCs display.

2. MATERIALS AND METHODS

2.1. Sample preparation

Ethics approval was granted by the Ryerson University Research and Canadian Blood Services Ethics Boards before the initiation of the study. The experiments were conducted using packed RBCs donated by healthy volunteers recruited by the Canadian Blood Services' Network Center for Applied Development (Vancouver, BC, CA). 1 ml of control blood sample and 1 ml of blood with 50 μM of C2-ceramide (Sigma Aldrich, ON, CA) were prepared to induce eryptosis [5]. The two vials were kept in an incubator at 37^{o}C and 280 RPM using Incu-Shaker (Benchmark Scientific, NJ, USA). After 24 hours a blood smear from each sample was prepared and investigated under an Olympus IX-71 optical microscope (Olympus Canada Inc., Markham, ON) attached to a CCD camera with a resolution of 1392 x 1040 pixels (Lumenera, Ottawa, CA). The images were acquired using a 100x oil immersion objective lens. The chromophore content of the control and ceramide induced samples were identified using a ABL-800 Flex blood gas analyzer (Radiometer Medical, London, CA). The changes in eryptotic RBCs were identified using a high frequency PA system and an integrating sphere.

2.2. PA signals acquisition

PA spectral analysis was tested on a vessel phantom prepared using a 10 % gelatin type A (Sigma Aldrich, ON, CA) and a metal rod of 0.5 mm in diameter. The vessel was located at a depth of 1 mm from the surface of the gelatin phantom. Images of the vessel phantom were then acquired using the commercial VevoLAZR system (Fujifilm,

Downloaded From: http://proceedings.spiedigitallibrary.org/ on 05/08/2016 Terms of Use: http://spiedigitallibrary.org/ss/TermsOfUse.aspx

Visual Sonics, Canada) attached to the LZ 550 transducer as shown in Figure 1a. The system is coupled to an OPO laser (Opotech North America Inc.) with a wavelength swept capability of 680 to 970 nm and an energy gradually decreasing from 30 to 20 mJ/pulse as a function of wavelength. Ten frames for each of the wavelengths 680, 710, 750, 800, 850, 900 nm were acquired. The PA signals were beamformed using delay and sum for every 64 elements. A representative beamformed image and PA radiofrequency signal acquired at 800 nm for the control sample is presented in Figure 1b, c.

Spectral analysis was performed on the normalized power spectra of PA signals. The power spectra were acquired from the top vessel boundary using a Hanning window. The resultant power spectra from different elements are presented in Figure 1d. The power spectra were normalized to a reference (Figure 1e) to reduce the effect of the transducer bandwidth on calculated spectral parameters [18], [21]. The reference sample was prepared using a 200 nm layer of gold mounted on top a microscopy slide with a 10 nm of chromium to strengthen the adhesion of the gold to the glass slide. The sample was prepared using a TES12D Thermal Evaporator which deposit thin metal films onto substrates using a thermal vapor deposition process (University of Toronto, Ontario, CA). Energy correction was applied to all the acquired signals.

The normalized power spectra were fitted to a straight line at the -6 dB bandwidth of the transducer (ranging between 10 to 45 MHz) using the mean square error as shown by a red line in Figure 1e with a regression value more than 0.9. The slope, y-intercept and MBF spectral parameters were derived from the fitted line for both the controlled and ceramide induced samples. The results were compared and correlated to morphological and biochemical changes in RBCs.

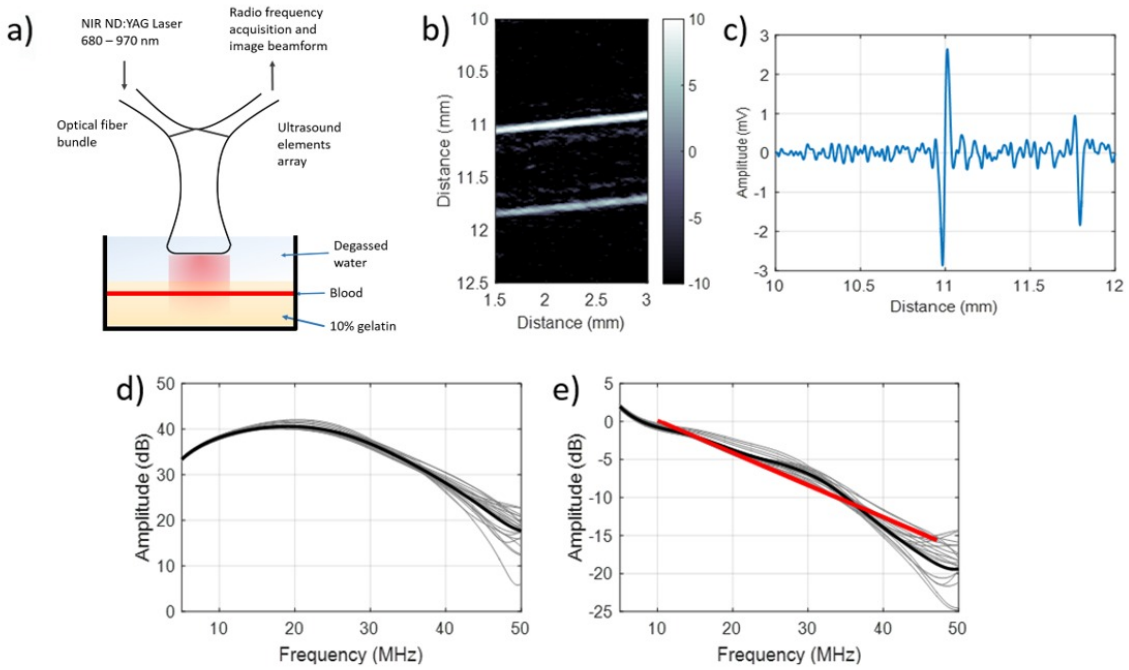

Figure 1: (a) Schematic representation of the VevoLAZR experimental setup. (b) A representative PA beamformed image of the vessel phantom at wavelength 800 nm of the control sample. (c) A representative radiofrequency beamformed PA signal. (d) and (e) are respectively the power spectra and normalized power spectra acquired using multiple elements. The bold black lines represent the average of the spectra. In (e) the red line represents the best-fit line at the sensitive range of the transducer.

Downloaded From: http://proceedings.spiedigitallibrary.org/ on 05/08/2016 Terms of Use: http://spiedigitallibrary.org/ss/TermsOfUse.aspx

2.3. Optical property measurements

The optical properties of the control and ceramide exposed blood samples were measured using a UV-Vis Spectrophotometer (Shimadzu Scientific Instrumentations, Columbian, MD) attached to an ISR-3100 integrating sphere. The integrating sphere and the optical beam were 60 mm and 8 mm in diameter, respectively. A sample holder with a short optical path of 200 µm cell in length was used (20/O-Q-0.2, Sterna, Atascadero, CA) [22]–[24]. Phosphate buffered saline (PBS) was used as a reference. The wavelength ranges were swept at 600 nm to 900 nm in increments of 2 nm.

Three different measurements were acquired to measure the total transmission, diffuse transmission and diffuse reflectance of the samples [22]–[24]. These measurements were used as an input to the inverse adding doubling (IAD) method with a refractive index set at 1.335. The wall reflectance of the sphere was measured and accounted for [25]. The outputs of the IAD method were the absorption, scattering and the anisotropy parameters of the samples. A comparative analysis between the spectrophotometer data and parameters acquired from PA spectral analysis was conducted.

3. RESULTS AND DISCUSSION

Optical images of the control and ceramide exposed RBCs are presented in Figure 2. The biconcave RBCs is the dominant morphology for the control sample. For the ceramide exposed sample membrane blebbing was present. This is expected as ceramide induces eryptosis which in turn, exhibits morphological changes such as membrane blebbing, cell shrinkage and membrane scrambling [11]. Chromophore contents measured using a blood gas analyzer are reported in Table 1. The results demonstrate an increase in deoxyhemoglobin and methemoglobin concentration by 1.34 and 2.81 respectively, and a decrease in oxyhemoglobin concentration by 1.07. The formation of methemoglobin has important roles in inflammation and vascular regulation [10], [26].

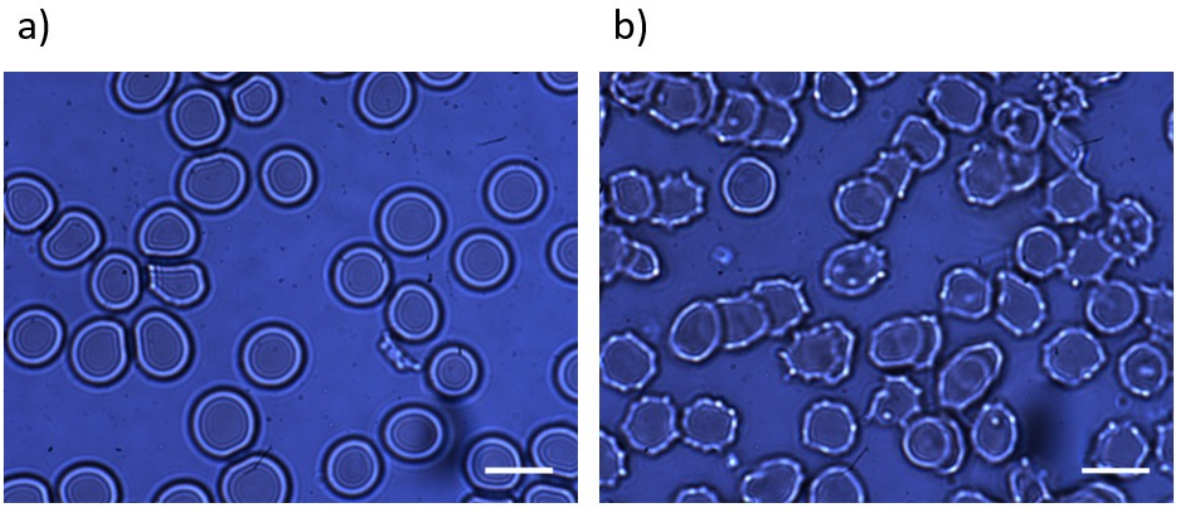

Figure 2: Optical images of RBCs acquired using inverted microscopy with 100x oil immerse lens. (a) Image of the control sample. (b) Image of the ceramide induced RBCs. Scale bar 10 µm.

Downloaded From: http://proceedings.spiedigitallibrary.org/ on 05/08/2016 Terms of Use: http://spiedigitallibrary.org/ss/TermsOfUse.aspx

Spectrophotometer measurements demonstrate changes in the optical properties because of adding ceramide (Figure 3). The absorption coefficient (Figure 3a) of the ceramide induced sample indicates the presence of methemoglobin peak at around 630 nm. This was expected due to the increase in the methemoglobin content that was independently verified using the blood gas analyzer (Table 1). Figure 3b shows the absorption coefficient for the selected wavelengths used in PA imaging (680 – 900 nm). The results demonstrate a decrease in the optical absorption coefficient from 0.08 mm^{-1} at 680 nm to 0.18 mm^{-1} at 900 nm for the ceramide induced sample. The scattering coefficient for the ceramide-induced sample decreased from 2.7 /mm at 680 nm to 3.3 /mm at 900 nm as shown in Figure 3c. The anisotropy coefficient increased from 0.07 at 680 nm to 0.05 at 900 nm (Figure 3d). The differences are presented in Figure 4.

	Oxyhemoglobin (%)	**Deoxyhemoglobin (%)**	**Methemoglobin (%)**	**sO_2 (%)**
Control	93.5	5.3	2.1	94.6
Ceramide	87.3	7.1	5.9	92.5

Table 1: Percent content of oxy-, deoxy-, methemoglobin and hemoglobin oxygen saturation (sO_2) as measured from the control and ceramide induced sample using a blood gas analyzer.

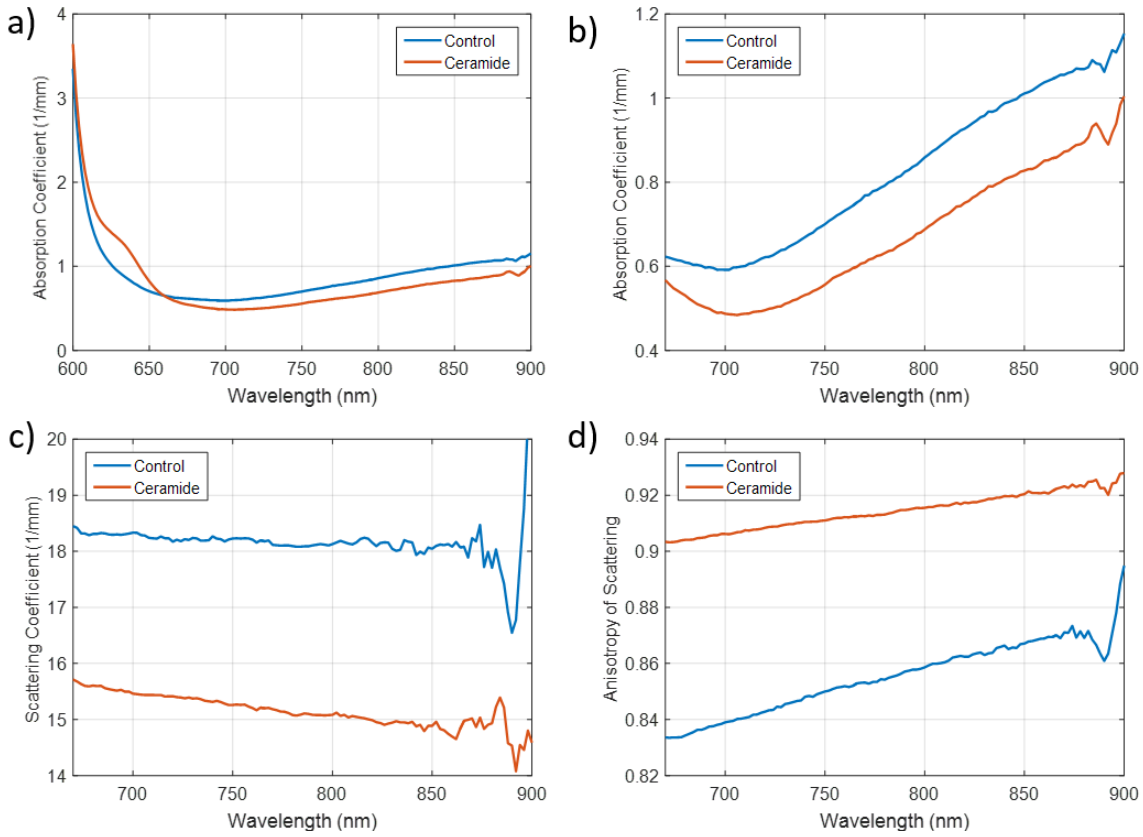

Figure 3: Spectrophotometer measurements from the control and ceramide exposed blood samples acquired using an integrating sphere. (a) The absorption coefficient calculated at the wavelengths 500 to 900 nm. (b) The absorption coefficient in (a), only between the selected wavelengths of 680 – 900 nm. (c) and (d) are the reduced scattering coefficient and the anisotropy factor.

Downloaded From: http://proceedings.spiedigitallibrary.org/ on 05/08/2016 Terms of Use: http://spiedigitallibrary.org/ss/TermsOfUse.aspx

The changes in the optical properties are due to the redistribution of hemoglobin molecules that occurs when RBCs undergo eryptosis. During eryptosis, a fraction of the hemoglobin molecules inside the RBCs will diffuse outside to the surrounding media resulting in a more homogeneous sample [10]. For high hematocrit samples such as the one used here, the detour effect is less pronounced as hemoglobin molecules diffuses outside RBCs [27], [28]. The detour effect is the increase in the optical path length (resulting in an increase in the scattering coefficient) due to increased refractions between and within the RBCs. The results for the optical properties are presented in Figure 3.

PA spectral parameters, the slope, y-intercept and MBF are presented in Figure 5. The ceramide induced sample reveal a non-significant increase in the spectral slope ($p>0.05$). The spectral slope parameter is associated with the absorber size [29]–[31], the increase of the spectral slope can be correlated to the reduction of the RBCs size as they undergo eryptosis (Cell shrinkage) [8], [15]. In addition, the PA spectral slope shows a significant decrease as a function of the optical wavelength. The wavelength dependant decrease in the spectral slope correlates to an increase in the absorber size, which can be linked to the increase in the optical wavelength sensitivity to oxyhemoglobin. Oxyhemoglobin is present in high concentration in the sample as measured using the blood gas analyzer (Table 1).

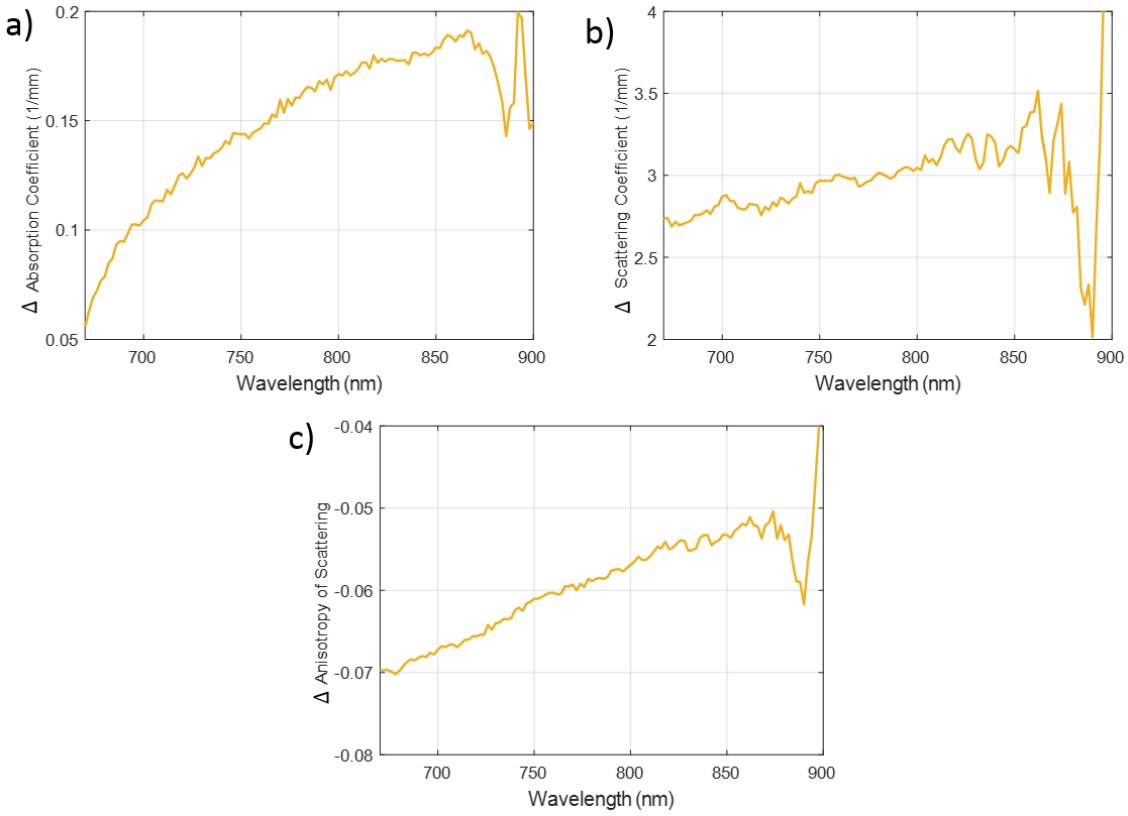

Figure 4: The change between the optical properties of the ceramide and the controlled sample presented in Figure 3. The difference in the absorption coefficient (a), the scattering coefficient (b) and the anisotropy coefficient (c).

For the y-intercept parameter, a significant decrease was observed at all the wavelengths. The y-intercept parameter is linked to changes in the concertation and distribution of the ultrasound source [30]–[32]. The changes in the distribution of hemoglobin reflect as an increase in the y-intercept (Figure 5b). This is expected as

Downloaded From: http://proceedings.spiedigitallibrary.org/ on 05/08/2016 Terms of Use: http://spiedigitallibrary.org/ss/TermsOfUse.aspx

the absorption coefficient of the control sample is higher than that of the ceramide exposed sample (Figure 3b). A significant decrease in the MBF for the ceramide induced sample was noted for the wavelengths 800, 850 and 900 nm. The MBF is a parameter that is dependent on both the slope and y-intercept.

These results suggest the capability of using PA spectral analysis in detecting changes in the distribution of chromophores, which occur in collection of RBCs undergoing eryptosis (biochemical and morphological changes). The results also suggest that PA spectral analysis can potentially be used to monitor vasculature collapse for cancer therapy. This is because when RBCs escape vascular compartments, they undergo eryptosis due to the stressful extravascular environment. The next step is to apply the spectral analysis tested above to wider ranges of wavelengths (< 680 nm) as the sensitivity to changes of damaged RBCs increase at lower wavelengths due to the formation of methemoglobin (Figure 3a). The organizational changes of chromophores within single RBC as it undergoes eryptosis have never been studied. Investigating these changes will result in better understanding of the changes in the spectral parameters.

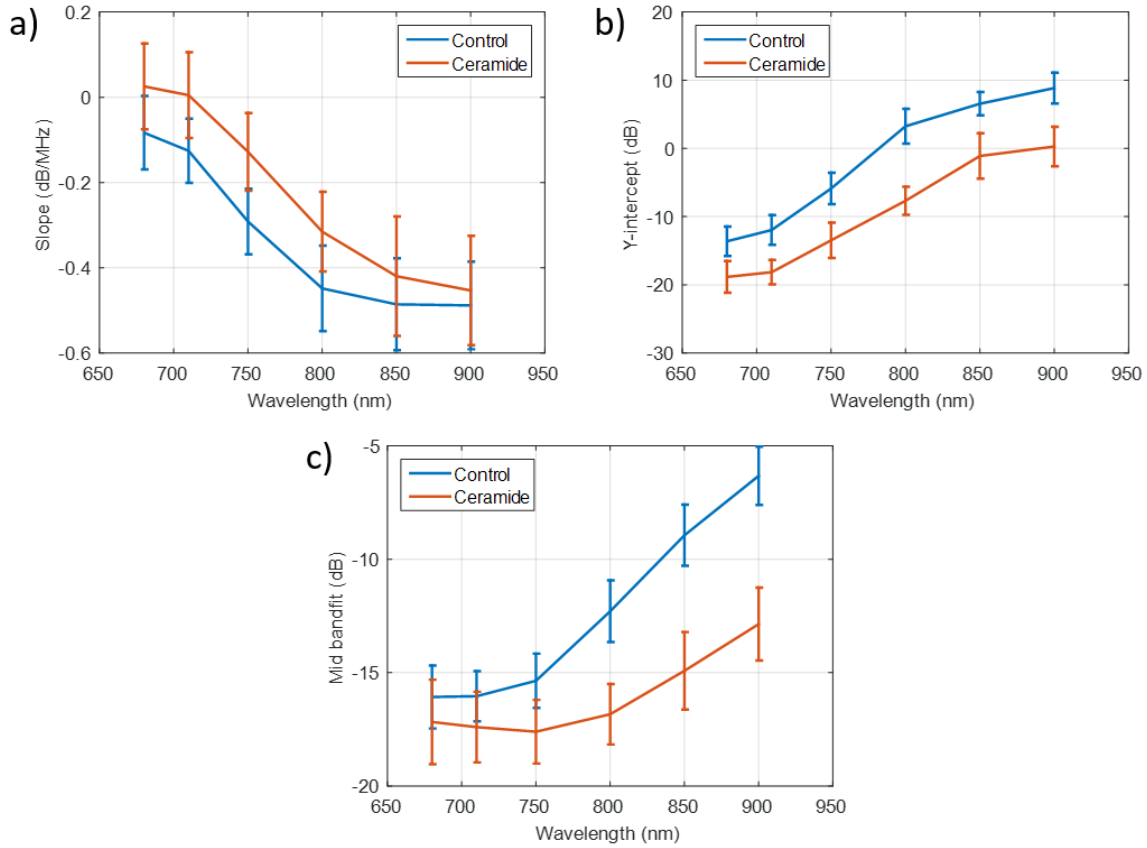

Figure 5: PA spectral parameters of the controlled and ceramide induced samples. (a), (b) and (c) are the slope, y-intercept and mid band-fit (MBF) spectral parameters calculated using the VevoLAZR system.

4. CONCLUSION

In this study, the potential of using high frequency PA spectral analysis in detecting changes in populations of RBCs as they undergo eryptosis has been examined. The changes in the populations of the different sizes of RBCs was reflected in the spectral slope measurements. The change in slope was statistically insignificant due to the minor

Downloaded From: http://proceedings.spiedigitallibrary.org/ on 05/08/2016 Terms of Use: http://spiedigitallibrary.org/ss/TermsOfUse.aspx

size differences between the control and the eryptotic cells. However, the y-intercept parameter demonstrates the highest sensitivity, at the wavelength ranges of 680 to 900 nm, for normal and eryptotic RBCs differentiation. The change in the y-intercept correlated to distribution of hemoglobin molecules as RBCs undergo eryptosis.

5. ACKNOWLEDGMENTS

We would like to thank Danielle Gifford for the helping with blood samples preparation and Eno Hysi for the help in using and analyzing the VevoLAZR data. The work was funded by the Natural Sciences and Engineering Research Council of Canada (NSERC) and Terry Fox Foundation (TFF) awarded to Michael C. Kolios.

6. REFERENCES

[1] W. T. Tran, S. Iradji, E. Sofroni, A. Giles, D. Eddy, and G. J. Czarnota, "Microbubble and ultrasound radioenhancement of bladder cancer," *Br. J. Cancer*, vol. 107, no. 3, pp. 469–476, Jul. 2012.

[2] G. J. Czarnota, R. Karshafian, P. N. Burns, S. Wong, A. A. Mahrouki, J. W. Lee, A. Caissie, W. Tran, C. Kim, M. Furukawa, E. Wong, and A. Giles, "Tumor radiation response enhancement by acoustical stimulation of the vasculature," *Proc. Natl. Acad. Sci.*, vol. 109, no. 30, pp. E2033–E2041, Jul. 2012.

[3] D. M. Skyba, R. J. Price, A. Z. Linka, T. C. Skalak, and S. Kaul, "Direct in vivo visualization of intravascular destruction of microbubbles by ultrasound and its local effects on tissue," *Circulation*, vol. 98, no. 4, pp. 290–293, Jul. 1998.

[4] D. L. Miller and J. Quddus, "Diagnostic ultrasound activation of contrast agent gas bodies induces capillary rupture in mice," *Proc. Natl. Acad. Sci. U. S. A.*, vol. 97, no. 18, pp. 10179–10184, 2000.

[5] J. T. Nofiele, R. Karshafian, M. Furukawa, A. Al Mahrouki, A. Giles, S. Wong, and G. J. Czarnota, "Ultrasound-activated microbubble cancer therapy: ceramide production leading to enhanced radiation effect in vitro," *Technol. Cancer Res. Treat.*, vol. 12, no. 1, pp. 53–60, Feb. 2013.

[6] P. Santana, L. A. Peña, A. Haimovitz-Friedman, S. Martin, D. Green, M. McLoughlin, C. Cordon-Cardo, E. H. Schuchman, Z. Fuks, and R. Kolesnick, "Acid sphingomyelinase-deficient human lymphoblasts and mice are defective in radiation-induced apoptosis," *Cell*, vol. 86, no. 2, pp. 189–199, Jul. 1996.

[7] S. Marathe, S. L. Schissel, M. J. Yellin, N. Beatini, R. Mintzer, K. J. Williams, and I. Tabas, "Human Vascular Endothelial Cells Are a Rich and Regulatable Source of Secretory Sphingomyelinase IMPLICATIONS FOR EARLY ATHEROGENESIS AND CERAMIDE-MEDIATED CELL SIGNALING," *J. Biol. Chem.*, vol. 273, no. 7, pp. 4081–4088, Feb. 1998.

[8] M. Föller, S. M. Huber, and F. Lang, "Erythrocyte programmed cell death," *IUBMB Life*, vol. 60, no. 10, pp. 661–668, Oct. 2008.

[9] F. Lang, E. Gulbins, H. Lerche, S. M. Huber, D. S. Kempe, and M. Foller, "Eryptosis, a window to systemic disease," *Cell. Physiol. Biochem. Int. J. Exp. Cell. Physiol. Biochem. Pharmacol.*, vol. 22, no. 5–6, pp. 373–380, 2008.

[10] J. Umbreit, "Methemoglobin--it's not just blue: a concise review," *Am. J. Hematol.*, vol. 82, no. 2, pp. 134–144, Feb. 2007.

[11] F. Lang, E. Gulbins, P. A. Lang, D. Zappulla, and M. Föller, "Ceramide in suicidal death of erythrocytes," *Cell. Physiol. Biochem. Int. J. Exp. Cell. Physiol. Biochem. Pharmacol.*, vol. 26, no. 1, pp. 21–28, 2010.

[12] L. Wang, K. Maslov, and L. V. Wang, "Single-cell label-free photoacoustic flowoxigraphy in vivo," *Proc. Natl. Acad. Sci. U. S. A.*, vol. 110, no. 15, pp. 5759–5764, 2013.

[13] M. Sivaramakrishnan, K. Maslov, H. F. Zhang, G. Stoica, and L. V. Wang, "Limitations of quantitative photoacoustic measurements of blood oxygenation in small vessels," *Phys. Med. Biol.*, vol. 52, no. 5, pp. 1349–1361, Mar. 2007.

Downloaded From: http://proceedings.spiedigitallibrary.org/ on 05/08/2016 Terms of Use: http://spiedigitallibrary.org/ss/TermsOfUse.aspx

[14] E. M. Strohm, M. J. Moore, and M. C. Kolios, “Single cell photoacoustic microscopy: a review,” *IEEE J. Sel. Top. Quantum Electron.*, vol. PP, no. 99, pp. 1–1, 2015.
[15] F. L. Lizzi, M. Greenebaum, E. J. Feleppa, M. Elbaum, and D. J. Coleman, “Theoretical framework for spectrum analysis in ultrasonic tissue characterization,” *J. Acoust. Soc. Am.*, vol. 73, no. 4, pp. 1366–1373, Apr. 1983.
[16] Y. Yang, S. Wang, C. Tao, X. Wang, and X. Liu, “Photoacoustic tomography of tissue subwavelength microstructure with a narrowband and low frequency system,” *Appl. Phys. Lett.*, vol. 101, no. 3, p. 034105, Jul. 2012.
[17] G. Xu, I. A. Dar, C. Tao, X. Liu, C. X. Deng, and X. Wang, “Photoacoustic spectrum analysis for microstructure characterization in biological tissue: A feasibility study,” *Appl. Phys. Lett.*, vol. 101, no. 22, p. 221102, Nov. 2012.
[18] E. Hysi, R. K. Saha, and M. C. Kolios, “Photoacoustic ultrasound spectroscopy for assessing red blood cell aggregation and oxygenation,” *J. Biomed. Opt.*, vol. 17, no. 12, p. 125006, Dec. 2012.
[19] R. E. Kumon, C. X. Deng, and X. Wang, “Frequency-domain analysis of photoacoustic imaging data from prostate adenocarcinoma tumors in a murine model,” *Ultrasound Med. Biol.*, vol. 37, no. 5, pp. 834–839, May 2011.
[20] G. Xu, Z.-X. Meng, J. D. Lin, J. Yuan, P. L. Carson, B. Joshi, and X. Wang, “The functional pitch of an organ: quantification of tissue texture with photoacoustic spectrum analysis,” *Radiology*, vol. 271, no. 1, pp. 248–254, Apr. 2014.
[21] R. K. Saha, S. Karmakar, E. Hysi, M. Roy, and M. C. Kolios, “Validity of a theoretical model to examine blood oxygenation dependent optoacoustics,” *J. Biomed. Opt.*, vol. 17, no. 5, p. 055002, May 2012.
[22] N. Bosschaart, G. J. Edelman, M. C. G. Aalders, T. G. van Leeuwen, and D. J. Faber, “A literature review and novel theoretical approach on the optical properties of whole blood,” *Lasers Med. Sci.*, vol. 29, no. 2, pp. 453–479, Mar. 2014.
[23] M. Friebel, A. Roggan, G. Müller, and M. Meinke, “Determination of optical properties of human blood in the spectral range 250 to 1100 nm using Monte Carlo simulations with hematocrit-dependent effective scattering phase functions,” *J. Biomed. Opt.*, vol. 11, no. 3, p. 34021, Jun. 2006.
[24] D. K. Sardar and L. B. Levy, “Optical Properties of Whole Blood,” *Lasers Med. Sci.*, vol. 13, no. 2, pp. 106–111, Jun. 1998.
[25] S. A. Prahl, M. J. C. van Gemert, and A. J. Welch, “Determining the optical properties of turbid media by using the adding–doubling method,” *Appl. Opt.*, vol. 32, no. 4, p. 559, Feb. 1993.
[26] S. N. Balaji and V. Trivedi, “Extracellular methemoglobin primes red blood cell aggregation in malaria: An in vitro mechanistic study,” *FEBS Lett.*, vol. 587, no. 4, pp. 350–357, Feb. 2013.
[27] A. T. Lovell, J. C. Hebden, J. C. Goldstone, and M. Cope, “Determination of the transport scattering coefficient of red blood cells,” 1999, vol. 3597, pp. 175–182.
[28] D. Yim, “CLBlood: A Cell-Based Light Interaction Model for Human Blood,” Jan. 2012.
[29] K. Nam, I. M. Rosado-Mendez, L. A. Wirtzfeld, A. D. Pawlicki, V. Kumar, E. L. Madsen, G. Ghoshal, R. J. Lavarello, M. L. Oelze, T. A. Bigelow, J. A. Zagzebski, W. D. O’Brien, and T. J. Hall, “Ultrasonic Attenuation and Backscatter Coefficient Estimates of Rodent-Tumor-Mimicking Structures: Comparison of Results among Clinical Scanners,” *Ultrason. Imaging*, vol. 33, no. 4, pp. 233–250, Oct. 2011.
[30] K. K. Shung and G. A. Thieme, *Ultrasonic Scattering in Biological Tissues*. CRC Press, 1992.
[31] J. Mamou and M. L. Oelze, Eds., *Quantitative ultrasound in soft tissues*. Dordrecht: Springer, 2013.
[32] K. P. Mercado, M. Helguera, D. C. Hocking, and D. Dalecki, “Estimating Cell Concentration in Three-Dimensional Engineered Tissues using High Frequency Quantitative Ultrasound,” *Ann. Biomed. Eng.*, vol. 42, no. 6, pp. 1292–1304, Jun. 2014.

Downloaded From: http://proceedings.spiedigitallibrary.org/ on 05/08/2016 Terms of Use: http://spiedigitallibrary.org/ss/TermsOfUse.aspx